

Article

Mineralogy of an Appinitic Hornblende Gabbro and Its Significance for the Evolution of Rising Calc-Alkaline Magmas

Georgia Pe-Piper 

Department of Geology, Saint Mary's University, Halifax, NS B3H 3C3, Canada; gpiper@smu.ca

Received: 3 November 2020; Accepted: 26 November 2020; Published: 3 December 2020



Abstract: The magmatic and sub-solidus evolution of calcic amphiboles and Fe–Ti oxides was investigated in the Neoproterozoic Frog Lake pluton, Nova Scotia, Canada, in order to understand the relationship between the history of hydrous magma and the resulting mineralogy. The pluton occurs as sheet-like bodies of hornblende gabbro and hornblendite, with lesser tonalite dykes and granite bodies, interlayered with screens of medium-grade metamorphic country rock. Small, diffuse clots of felsic minerals are present in the gabbro. The subsolidus growth of actinolite occurs in early clinopyroxenes and amphiboles. Ilmenite is the dominant Fe–Ti oxide, as interstitial magmatic crystals. The increase of Mn towards the margin of the ilmenite crystals indicates a gradual increase in oxygen fugacity with time, leading to the precipitation of titanite and ferrohypersthene. The replacement of titanite by ilmenite and ilmenite lamellae in the amphiboles suggests subsequent reducing conditions during the sub-solidus crystallisation. The gabbros in the coeval, but apparently shallower, Jeffers Brook granodiorite laccolith have dominant magnetite and Mg-rich subsolidus amphiboles, which are indicative of high oxygen fugacity. The differences between the two plutons suggest that there was a greater flux of hydrothermal water through the sheet-like architecture of the Frog Lake pluton.

Keywords: amphibole; hornblende; pargasite; actinolite; ilmenite; magnetite; gabbro

1. Introduction

Amphiboles and iron-titanium oxides are important indicators of the evolution of hydrous magmas that build calc–alkaline intrusive complexes. The crystallisation of amphiboles from mafic magmas has an important buffering effect on the concentration of dissolved water in the magma, and thus on oxygen fugacity. The physical conditions of the crystallisation and the degree of openness of the system may thus have an important influence on the evolution of the magma, the composition of minerals that crystallise from it, and the production of hydrothermal fluids [1].

In the Avalon terrane of northern mainland Nova Scotia, Canada (Figure 1), calc–alkaline hornblende gabbro to granodiorite plutons, resembling appinites, were emplaced at 620 to 605 Ma [2]. Three appinite complexes are well known in Nova Scotia: the Frog Lake pluton [3,4] and the Jeffers Brook pluton [5] in the Cobequid Highlands, and the Greendale complex in the Antigonish Highlands [6] (Figure 1a). The Greendale complex was emplaced in a dextral fault zone into greenschist to sub-greenschist Neoproterozoic country rock [7]. The Frog Lake and Jeffers Brook plutons represent strongly-contrasting styles and depths of emplacement. The Jeffers Brook pluton was emplaced as a laccolith with a gabbroic floor at an upper crustal structural level into Neoproterozoic supracrustal rocks of lower greenschist facies [5].

The present study investigates the mineralogy of the Frog Lake hornblende gabbro pluton [4], which was emplaced into upper greenschist Mesoproterozoic country rock including biotite–quartz–chlorite–garnet schists [8]. Most plutonic rocks are hornblende gabbro, and some

hornblendite in which the framework of the rock is dominated by amphibole crystals. The pluton in general consists of sub-vertical sheet-like igneous bodies with irregular margins. The gabbro is cut by irregular dykes of tonalite, some of which show syn-magmatic deformation (Figure 1d). The thin gabbro sheets interleaved with the country rock are highly strained (Figure 1f). The emplacement of the Frog Lake gabbro was in a deforming strike-slip fault zone, with room created by local transtension. Where the outcrop is sufficient, the gabbro is not more than 100 m wide between the host-rock screens, and thus did not expand to the normal plutonic dimensions [4].

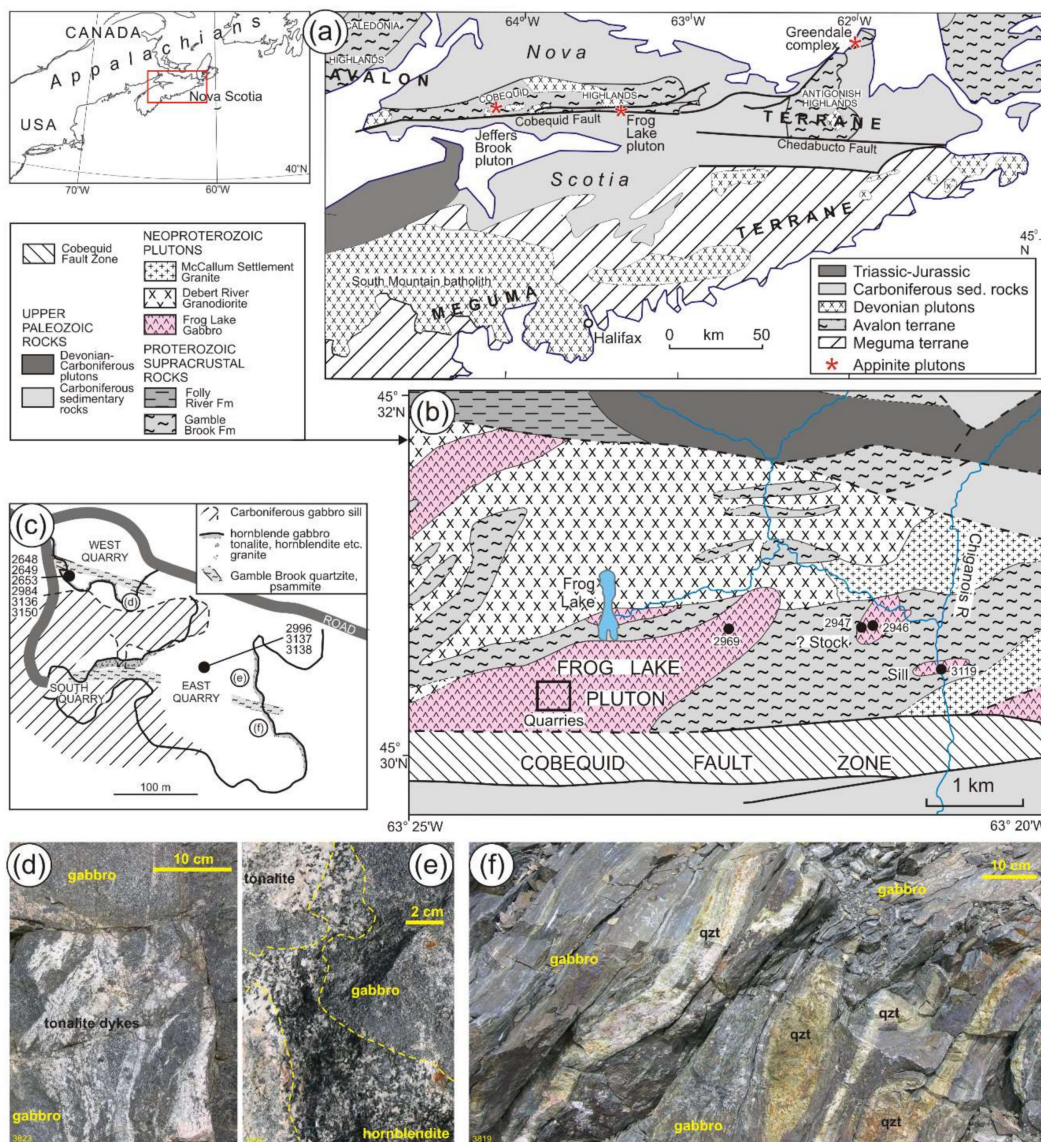


Figure 1. (a) Location map of the appinitic plutons in the Avalon terrane of Nova Scotia. The inset shows the location in eastern Canada. (b) Geological map of the Frog Lake pluton modified from Pe-Piper and Piper [3]. The rocks of the Cobequid Fault zone include sheared equivalents of rocks to the north; south of the Cobequid Fault zone, there are Carboniferous sedimentary rocks. Most of the analysed samples are from the quarries; other sample numbers are indicated on the map (solid circles). (c) Map of the Frog Lake quarries. This also shows the locations of samples and photographs (d–f). (d) Synmagmatic deformation of tonalite dykes in gabbro. (e) Gabbro with hornblendite and tonalite dykes. (f) Sheets of foliated gabbro between screens of quartzite.

The purpose of this paper is to investigate, in detail, the chemical mineralogy of the gabbros of the Frog Lake pluton, and to understand the relationship between the fluid evolution and the detailed amphibole and Fe–Ti oxide chemistry. This pluton has a well-preserved sheet-like structure, and appears to have been constructed sequentially by small magma batches. A comparison will be made with the chemical mineralogy of the amphiboles in the Jeffers Brook laccolith [9], with a very different style of pluton construction at a higher level in the crust, from magmas which are chemically similar to those in the Frog Lake pluton.

2. Geological Setting

The Late Neoproterozoic Frog Lake hornblende gabbro pluton intrudes into the Avalon terrane metasedimentary rocks. It consists of a main pluton outcropping of over 4 km², and smaller stocks and sheets of gabbro (Figure 1b). The pluton outcrops on the Cobequid Highlands plateau immediately north of the Cobequid Fault, a major strike slip fault that was active in the Devonian and Carboniferous. The best exposures are in rock quarries (Figure 1c) and in the deeply-incised Chiganois River valley; scattered outcrops also occur in areas where the glacial drift cover is thin. The pluton intrudes into the Mesoproterozoic Gamble Brook Formation (metaquartzites, psammites and pelites) in subvertical sheets (Figure 1f). ⁴⁰Ar/³⁹Ar geochronology on hornblende [2] yielded an age of 622 ± 3 Ma. The pluton is intruded by granite that is correlated with the McCallum Settlement granite, dated at 575 ± 22 Ma [10].

On the outcrop scale, the hornblende gabbro is inhomogeneous (Figure 1e), with pervasive irregular dyking by different gabbroic phases, oriented phenocrysts, and irregular dykes of tonalite, with evidence of syn-magmatic deformation (Figure 1d). Lateral contacts with country rock and xenoliths of psammite show the local metasomatic growth of hornblende. The pluton near the country rock includes pegmatites of both hornblende (Figure 1e) and granite. Geochemical analyses [4] have shown two types of hornblende gabbro, distinguished by their TiO₂ content. The low-Ti hornblende gabbros have trace element abundances similar to subduction-related mafic rocks, including enrichment in large-ion lithophile elements (LILE), and marked relative depletion in Nb and Y. The high-Ti hornblende gabbros (including pyroxene–mica gabbro) show more alkaline characteristics, with relatively higher amounts of Na₂O, P₂O₅, Nb, Y, light rare earth elements (REE) and high field strength elements (HFSE). The magmas that formed the Frog Lake pluton were very hydrous, resulting in the abundance of amphibole and mica.

The Jeffers Brook pluton [5] is a laccolith of a slightly younger age [2], situated about 80 km west of the Frog Lake pluton (Figure 1a). The Jeffers Brook pluton consists mainly of tonalite–granodiorite, but the base of the laccolith and the underlying sills include gabbro, hornblende gabbro and diorite, and similar hornblende gabbro occurs as discrete bodies and enclaves in the main tonalite–granodiorite. The more mafic phases show some alkaline characteristics—such as relatively high Ti, Zr, Y and Nb—but are geochemically similar to the low-Ti hornblende gabbros in the Frog Lake pluton. The Jeffers Brook pluton was emplaced at a higher structural level than the Frog Lake pluton, based on the grade of metamorphism of the country rock and the regional abundance of supracrustal rocks.

3. Petrography

The dominant hornblende gabbro of the Frog Lake pluton [4] comprises principally anhedral plagioclase grains and stubby amphibole in an interlocking lattice with interstitial biotite, quartz, and alkali feldspar. The equigranular, plagioclase–phyric, and pyroxene–mica–phyric hornblende gabbros have sub-equal amounts of amphibole and plagioclase. In hornblende, the framework of the rock is dominated by amphibole crystals. All of the pyroxene–mica–phyric gabbro and some of the equigranular and plagioclase–phyric gabbros have high Ti, and contain more ilmenite, titanite, biotite, clinopyroxene and apatite compared to the low-Ti suite. Cumulate clots or enclaves of amphibole and plagioclase crystals are widespread. Felsic mineral clots are common in some gabbros, consisting of quartz, albitised plagioclase and K-feldspar in diffuse centimetre-scale patches.

Amphibole makes up 50% to 80% of the rocks, occurring as individual anhedral crystals, as aggregates, and as overgrowths or replacements of clinopyroxene or orthopyroxene. The opaque oxide minerals are principally ilmenite and magnetite. The interstitial minerals include highly-chloritised biotite, orthoclase, quartz, titanite, calcite, pyrite and chalcopyrite. The pyroxene–mica gabbro consists of albitised plagioclase, clinopyroxene, biotite, and opaque minerals, with less-abundant amphibole.

Tonalite–granodiorite dykes comprise small plagioclase phenocrysts with interstitial anhedral quartz, K-feldspar, and accessory magnetite, biotite, chlorite and apatite. The felsic rocks associated with the gabbro near the country rock include granitic pegmatite and leucogranite that are mineralogically and chemically distinct from the felsic rocks of the nearby Debert River and McCallum Settlement plutons (Figure 1b; [11]), and have been shown to be strongly influenced by the metasomatism of country rock [4]. The xenoliths of psammite contain large amphibole porphyroblasts (some replaced by actinolite) within 1 cm of the igneous contact. Whole rock geochemical analysis has shown that these xenoliths are enriched in MgO and depleted in TiO₂, P₂O₅, Nb, Rb, Zr, Sr and Ba compared with the psammite a few metres from the contact [4]. The hornblendite that envelopes these xenoliths is, in most places, pegmatitic and transitions into gabbro. Titanite is abundant in some hornblendite pegmatites near the contact, both as inclusions in amphibole crystals and as large independent crystals, and has also been noted in the felsic pegmatites.

4. Materials and Methods

Twelve representative samples were selected for detailed study: three high-Ti-hornblende gabbros, one low-Ti-hornblende gabbro, two hornblendites, one pegmatitic hornblendite, one pyroxene–mica gabbro, two small felsic bodies, and two metasomatised psammite samples. The samples were examined by optical microscopy, and the amphiboles from six of the samples were analysed by electron microprobe (Table 1).

Table 1. Representative analyses of the amphibole by electron microprobe.

Analysis Sample Mineral Location	Low-Ti Hornblende Gabbro				High-Ti Hornblende Gabbro				Hornblendite			
	1 C3137 Hbl ¹ core	2 C3137 A-Hbl rim	3 C3137 Hbl core	4 C3137 Hbl rim	5 C2969 P-Hbl core	6 C2969 A-Hbl core	7 C9697 Hbl rim	8 C2969 P-Hbl core	9 C2969 Act rim	10 C3138 Hbl	11 C3138 Hbl	12 C3138 Act
SiO ₂	49.59	50.61	45.4	44.69	42.95	49.59	44.89	42.34	53.38	45.87	47.92	53.48
TiO ₂	0.33	0.28	1.81	1.78	2.58	0.67	1.34	1.65	0.25	1.56	0.65	0.1
Al ₂ O ₃	5.74	4.96	8.8	9.01	10.36	4.73	7.43	9.7	1.96	9.38	7.22	0.62
FeO _t	13.69	13.05	13.89	14.55	15.7	13.98	14.82	17.29	12.52	13.32	14.44	18.33
MnO	0.34	0.44	0.25	0.29	0.37	0.31	0.4	0.25	0.35	0.32	0.26	0.86
MgO	14.74	15.18	13.07	12.17	10.63	14.28	12.26	10.53	16.02	12.99	12.96	14.95
CaO	11.57	11.45	11.67	11.69	11.83	12.3	11.58	11.94	12.84	11.45	12.59	7.17
Na ₂ O	0.72	0.64	1.04	0.95	1.57	0.59	1.11	1.37	0.27	1.04	0.83	0.07
K ₂ O	0.22	0.16	0.75	0.66	0.92	0.42	0.81	1.15	0.13	0.64	0	0
Total	96.94	96.77	96.68	95.79	96.91	96.87	94.64	96.22	97.72	96.57	96.87	95.58
Structural formulae on the basis of 23 oxygen atoms and 13 cations												
Si	7.14	7.26	6.67	6.66	6.46	7.25	6.81	6.45	7.67	6.71	7.04	8.00
Ti	0.04	0.03	0.20	0.20	0.29	0.07	0.15	0.19	0.03	0.17	0.07	0.01
Al ^{IV}	0.86	0.74	1.33	1.34	1.54	0.75	1.19	1.55	0.33	1.29	0.96	0.00
Al ^{VI}	0.11	0.10	0.20	0.25	0.30	0.07	0.14	0.19	0.00	0.33	0.29	0.10
Fe ³⁺	0.87	0.85	0.62	0.56	0.20	0.44	0.49	0.47	0.23	0.62	0.34	0.00
Fe ²⁺	0.78	0.72	1.09	1.25	1.77	1.27	1.39	1.74	1.27	1.01	1.44	2.29
Mn	0.04	0.05	0.03	0.04	0.05	0.04	0.05	0.03	0.04	0.04	0.03	0.11
Mg	3.16	3.25	2.86	2.70	2.38	3.11	2.77	2.39	3.43	2.83	2.84	3.33
Ca	1.78	1.76	1.84	1.87	1.91	1.93	1.88	1.95	1.98	1.79	1.98	1.15
Na	0.20	0.18	0.30	0.27	0.46	0.17	0.33	0.40	0.08	0.29	0.24	0.02
K	0.04	0.03	0.14	0.13	0.18	0.08	0.16	0.22	0.02	0.12	0.00	0.00
Thermobarometric estimates from Ridolfi et al. (2010)												
P (MPa)	78	64	172	187	270	62	-	235	31	197	-	-
±	9	7	19	21	30	7	-	26	8	49	-	-
T (°C)	753	739	850	852	900	742	-	888	674	848	793	-
±	22	22	22	22	22	22	-	22	22	22	56	-

Table 1. Cont.

	Pegmatitic Hornblendite				Px-Mica Gabbro				Metasomatised Psammite			
Analysis	13	14	15	16	17	18	19	20	21	22	23	24
Sample	C2653	C2653	C2653	C2653	C2653	C2653	C2947	C2947	C2649	C2649	C2649	C2649
Mineral	A-Hbl	Act	A-Hbl	Hbl	Hbl	Act	E-Arf	FeAct	P-Hbl	Hbl	Act	Act
Location	host	lam.	lam.									
SiO ₂	51.9	53.78	50.84	47.15	46.18	50.41	47.51	48.06	43.01	47.24	51.83	52.89
TiO ₂	0.33	0.2	0.35	0.43	0.18	0	2.87	0.25	2.66	2.08	0.56	0.12
Al ₂ O ₃	3.47	2.94	3.86	6.82	8.71	1.06	2.23	0.88	10.81	7.35	4.91	2.62
FeO _t	11.34	10.7	11.02	13.31	14.12	16.47	27.77	33.79	11.44	9.57	7.11	9.61
MnO	0.1	0.15	0.18	0.27	0.2	0.13	0.56	1.23	0.22	0.38	0.22	0.24
MgO	16.12	17.15	16.02	13.95	13.06	12.78	3.97	2.88	12.66	14.49	16.94	15
CaO	12.85	12.55	12.64	11.65	11.97	12.78	5.01	7.18	12.7	13.49	12.58	13.96
Na ₂ O	0.39	0.28	0.42	0.69	0.99	0.14	4.7	0.43	1.31	0.48	0.8	0.34
K ₂ O	0.04	0.01	0	0.14	0.09	0	1.1	0.15	0.89	0.3	0.32	0.11
Total	96.54	97.76	95.33	94.41	95.5	93.77	95.72	94.85	95.7	95.38	95.27	94.89
Structural formulae on the basis of 23 oxygen atoms and 13 cations												
Si	7.51	7.60	7.43	6.99	6.82	7.69	7.54	7.96	6.47	7.03	7.53	7.93
Ti	0.04	0.02	0.04	0.05	0.02	0.00	0.34	0.03	0.30	0.23	0.06	0.01
Al ^{IV}	0.49	0.40	0.57	1.01	1.18	0.31	0.46	0.04	1.53	0.97	0.47	0.07
Al ^{VI}	0.10	0.09	0.10	0.18	0.34	-0.11	-0.04	0.12	0.39	0.32	0.38	0.40
Fe ³⁺	0.21	0.40	0.31	0.80	0.72	0.06	0.00	0.00	0.00	0.00	0.00	0.00
Fe ²⁺	1.16	0.87	1.04	0.85	1.03	2.04	3.69	4.68	1.44	1.19	0.86	1.21
Mn	0.01	0.02	0.02	0.03	0.03	0.02	0.08	0.17	0.03	0.05	0.03	0.03
Mg	3.48	3.61	3.49	3.08	2.88	2.91	0.94	0.71	2.84	3.21	3.67	3.35
Ca	1.99	1.90	1.98	1.85	1.89	2.09	0.85	1.27	2.05	2.15	1.96	2.24
Na	0.11	0.08	0.12	0.20	0.28	0.04	1.45	0.14	0.38	0.14	0.23	0.10
K	0.01	0.00	0.00	0.03	0.02	0.00	0.22	0.03	0.17	0.06	0.06	0.02
Thermobarometric estimates from Ridolfi et al. (2010)												
P (MPa)	45	39	-	-	-	-	-	-	-	-	-	-
±	5	4	-	-	-	-	-	-	-	-	-	-
T (°C)	713	695	-	-	826	-	-	-	-	-	-	-
±	22	22	-	-	56	-	-	-	-	-	-	-

Although the analyses with totals outside the range 96.5 to 98.5% were normally not used, they are shown here where they are the only analysis to illustrate a particular feature. Hbl: hornblende; A-Hbl: actinolitic hornblende; P-Hbl: pargasitic hornblende; Act: actinolite; lam.: twin lamellae; FeRct: ferrichterite; FeAct: ferroactinolite.

The analyses were made using a JEOL-733 electron microprobe with four wavelength spectrometers and a Tracor Northern 145-eV energy-dispersive detector. The operating conditions were 15 kV with a 5 nA beam current. The data were reduced using a Tracor Northern matrix correction program, with geological standards. The analyses of the amphiboles with totals outside the range of 96.5% to 98.5% were rejected as being of poor quality. Many of the actinolite analyses showed totals of less than 96%. The structural formulae for the remaining analyses were recalculated in order to distribute the ferric and ferrous iron on the stoichiometric basis of the sum of the cations of Ca, Na and K being 13 [12], using the software of Ridolfi et al. [13]. The same software was used to estimate the pressure and temperature of the crystallisation.

5. Results: Amphiboles

5.1. Optical and Chemical Classification of the Amphiboles

Six types of amphibole were distinguished on the basis of their colour in plane-polarised light and their chemical composition (Figure 2; [14]). They are:

1. brown pargasite (to pargasitic edenite) (e.g., analysis 5, Table 1);
2. olive green magnesiohornblende (e.g., 7, Table 1).
3. light green actinolitic hornblende (using the nomenclature of [15]; e.g., 2, Table 1);
4. almost-colourless actinolite (e.g., 9, Table 1);
5. rare dark green ferroactinolite (e.g., 20, Table 1);
6. rare blue-green ferrichterite (sodic-calcic amphibole).

The high-Ti hornblende gabbro contains pargasite, magnesiohornblende, actinolitic hornblende and actinolite (Figure 2). Ferrichterite and ferroactinolite are only found in the pyroxene–mica gabbro.

The low-Ti hornblende gabbros and most of the hornblendites contain only magnesiohornblende and actinolitic hornblende; there is also abundant actinolite in the pegmatitic hornblendite. The contact-metasomatised psammites contain large porphyroblasts of magnesio-hornblende and pargasite, and smaller crystals of actinolite (analyses 21–24, Table 1).

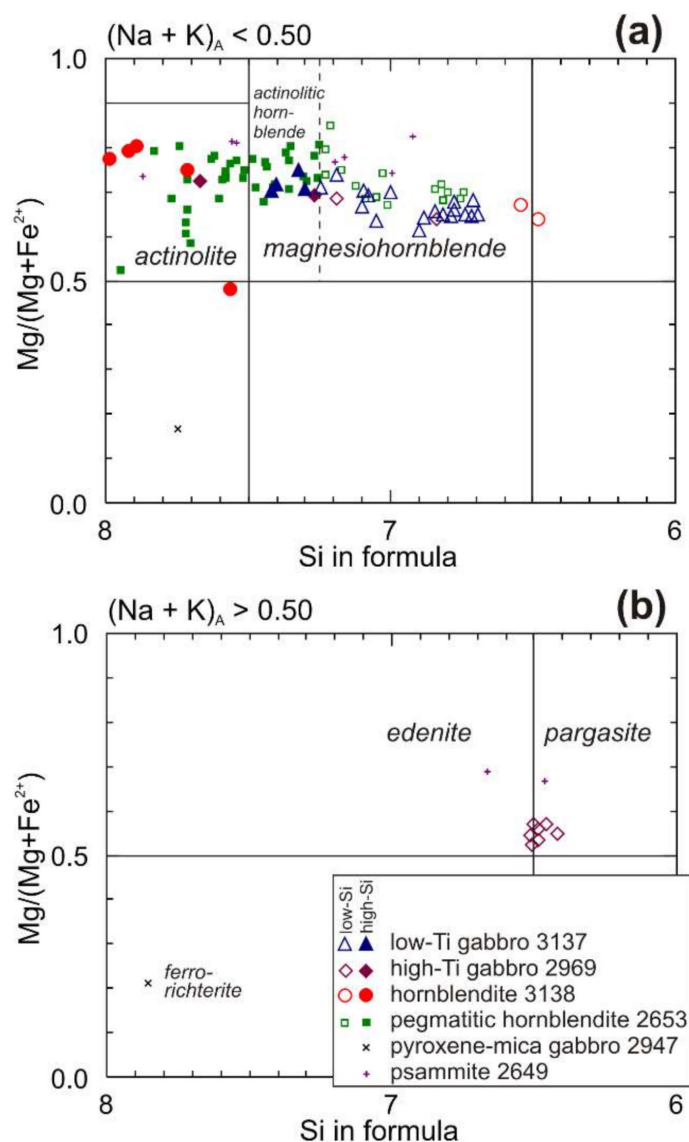


Figure 2. Plots showing the chemical classification (according to [14]) of the amphibole compositions for high-Ti gabbro, low-Ti gabbro, hornblendite, pegmatitic hornblendite and metasomatised psammite. The open symbols correspond to amphiboles with Si < 7.25 (hornblende and pargasite), and the solid symbols correspond to amphiboles with Si > 7.25 (actinolitic hornblende and actinolite). (a) shows amphiboles with $(\text{Na} + \text{K})_A < 0.5$, (b) > 0.5 .

The analyses of the amphibole from the pegmatitic hornblendite and the metasomatised psammites show substantial scatter in the abundance of most elements, with some very high Ti values in the porphyroblasts in the psammite xenoliths (Figure 3a).

The plots of the elements as cations vs. Si (Figure 3) indicate that, during the progressive crystallization, there was an increase in Mg, and a decrease in Na, K, Fe, and Ti. The concentration of the Ca remained almost constant, whereas there is scatter in the ^{VI}Al and Mn.

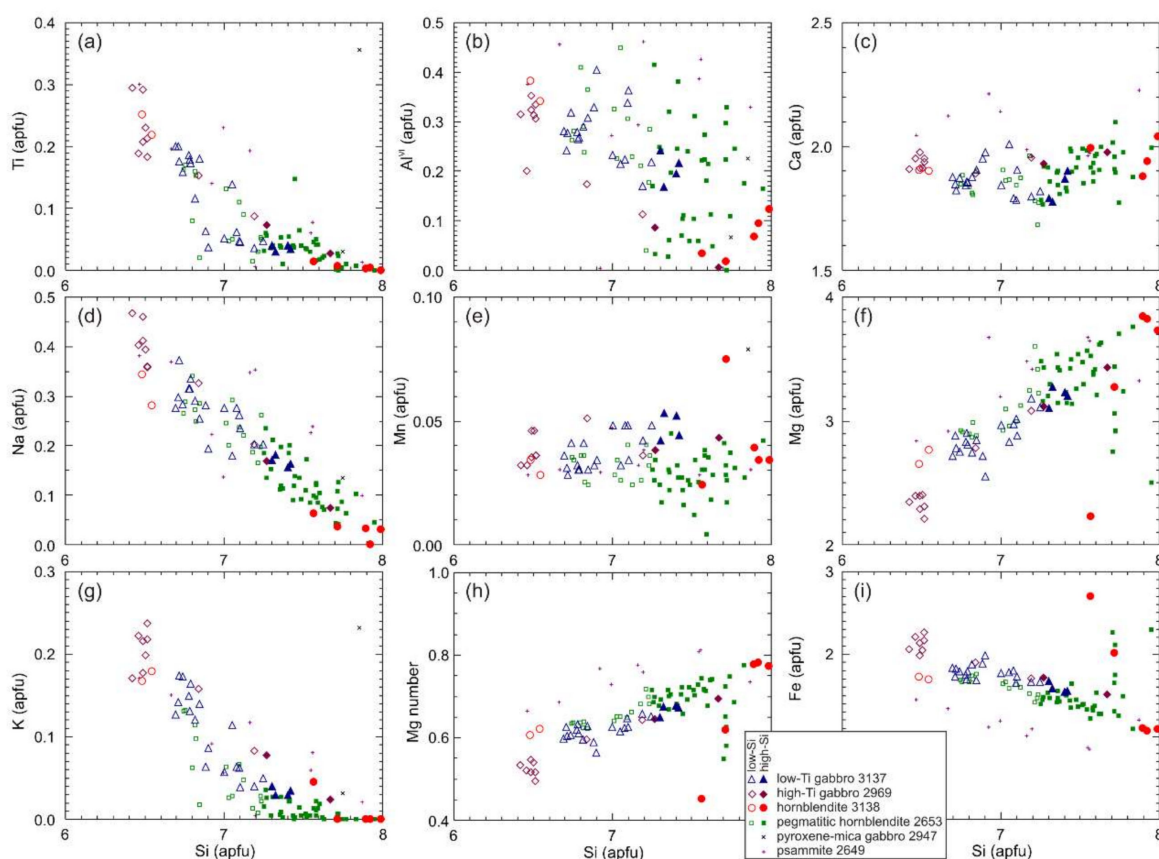


Figure 3. Cation variations with Si for the analysed amphiboles (based on 23 oxygens). (a) is Ti; (b) is Al^{vi} ; (c) is Ca; (d) is Na; (e) is Mn; (f) is Mg; (g) is K; (h) is Mg/(Mg+Fe); (i) is Fe.

5.2. Textural Relationships of the Amphiboles

The commonly-occurring textural relationships between the various amphiboles is that pargasite is overgrown by green magnesiohornblende or actinolitic hornblende, and the green magnesiohornblende is overgrown by light green actinolitic hornblende. The actinolitic hornblende overgrowths show a uniform optical orientation, and where the rocks are fractured shows no relation to those fractures. Some hornblende crystals poikilitically enclose clinopyroxene (Figure 4a) and orthopyroxene; others enclose pseudomorphs of actinolite with the external morphology of clinopyroxene (Figure 5a).

The other hornblende crystals have a hollow core (Figure 4b), or cores consisting of albite or partly-recrystallised quartz. Many of the hornblende crystals have a core of somewhat fibrous actinolite which, in some cases, has a distinct preferred orientation (Figure 4c), and may be twinned (Figure 4c); the other crystals consist of a mass of subparallel prismatic actinolite which appears to interdigitate with hornblende. Other green hornblende crystals contain some areas of secondary actinolite, or are rimmed by light green actinolite. The light green actinolite (13, Table 1) contains small subparallel prismatic actinolitic hornblende–actinolite crystals (perhaps twin lamellae; 14, 15, Table 1) similar to those that developed in hornblende.

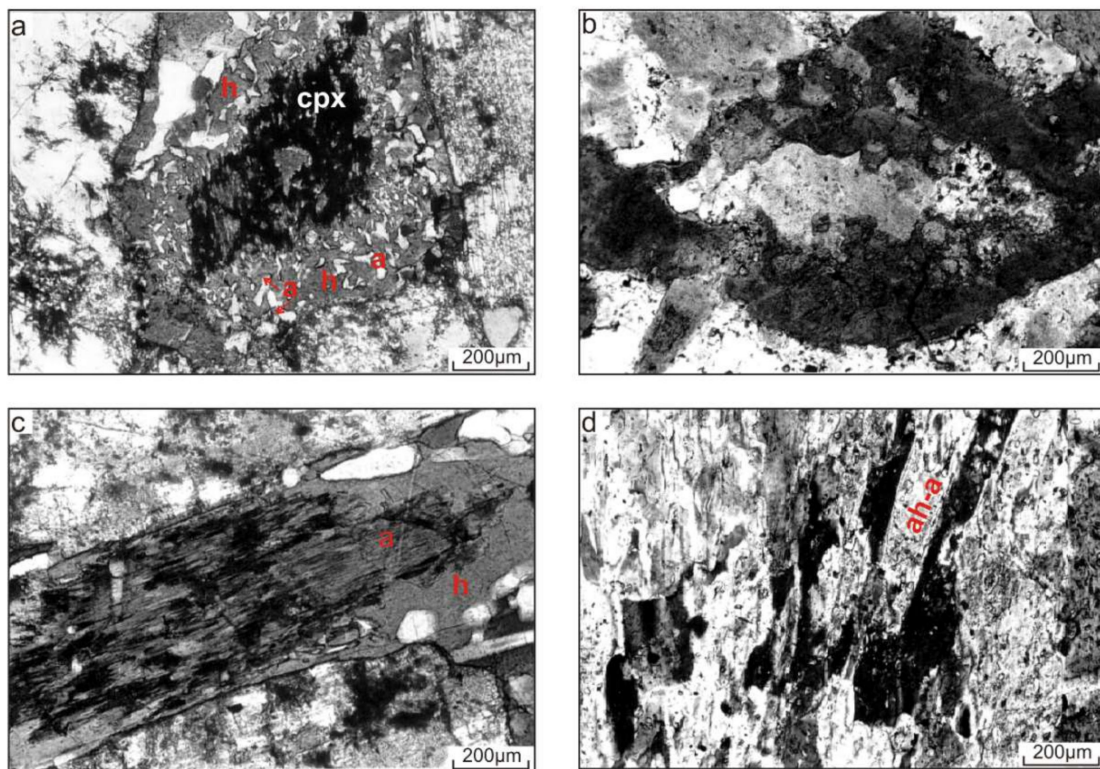


Figure 4. Petrographic microscope photomicrographs illustrating the textural relationships in the amphiboles. a: actinolite; ah: actinolitic hornblende; cpx: clinopyroxene; h: hornblende. Each field of view is approximately 2.5 mm. (a) Altered clinopyroxene forming the core of an olive-green to pale brown hornblende. Actinolite vermicules radiate from the core. High-Ti hornblende gabbro 2946, crossed polars. (b) Amphiboles with hollow cores. Pegmatitic hornblendite 2653, plane-polarised light. (c) Amphibole crystal with core of fibrous actinolite (pseudomorphing clinopyroxene) rimmed by olive-green hornblende. High-Ti hornblende gabbro 2946, plane polarised light. (d) Actinolite with twins or inclusions of actinolitic hornblende–actinolite. Pegmatitic hornblendite 2653, crossed polars (cf. analyses 13–15, Table 1).

Some high-Ti hornblende gabbros from the quarry sections show multiple phases of amphibole crystallisation, perhaps mirroring—on a microscopic scale—the dyking evident at the outcrop scale. Gabbro sample 3150 is cut by hornblendite dykes (Figure 6b) with chilled margins that are made up almost entirely of amphibole, ilmenite and magnetite, with 5–10 µm quartz and possibly feldspar crystals. The amphibole in the dyke includes large brown pargasite crystals (e.g., spots 4, 5, 9) similar to those in the host rock, with actinolite rims (e.g., spots 14, 3), all set in an aggregate of hornblende and actinolite laths. The host gabbro contains a few large brown pargasite crystals (< 5 mm) with hackly margins and patches of actinolite (Figure 6a): these large crystals (spots 16, 6) are surrounded by small prisms of hornblende (spots 22, 17).

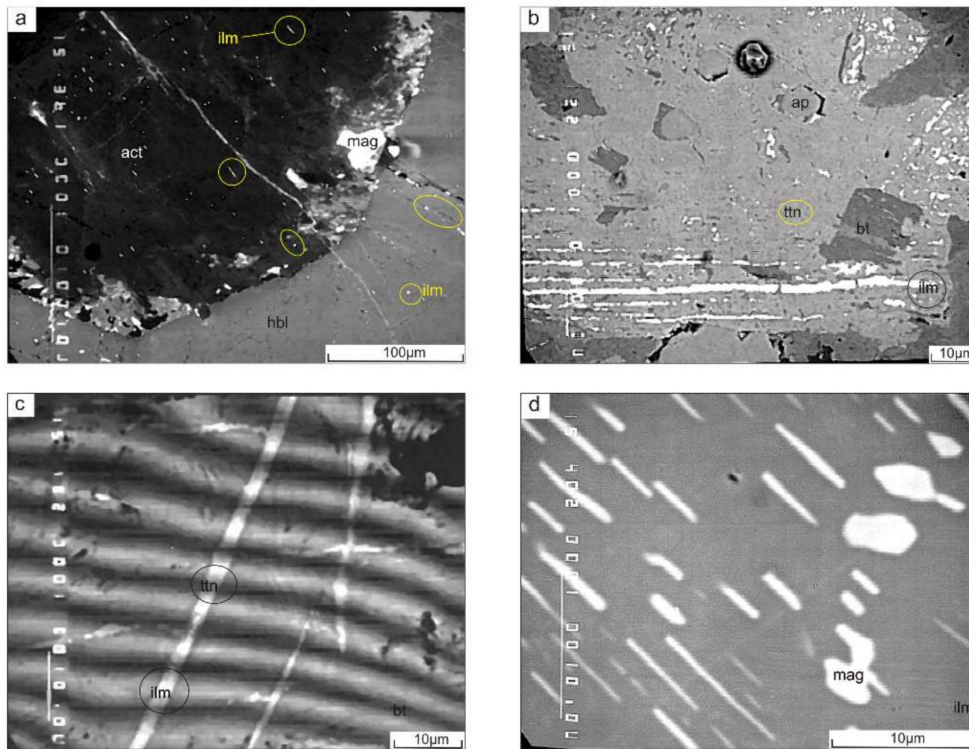


Figure 5. Backscattered electron (electron microprobe) images showing the textural relationships of the minerals. act: actinolite, ap: apatite, bt: biotite, ilm: ilmenite, mag: magnetite, ttn: titanite. (a) Actinolite (pseudomorphing clinopyroxene) poikilitically-enclosed by hornblende with rod-like bodies of ilmenite in both actinolite and hornblende. Inclusions of magnetite occur along the reaction zone between the actinolite and the hornblende. Hornblendite 3138. (b) titanite crystal(s) with inclusions of apatite and biotite–chlorite and lamellae, and patches of ilmenite (Pyroxene–mica gabbro 2947) (cf. analyses 24, 25 in Table 2). (c) Partly-chloritised biotite traversed by opaque bars of titanite with small patches of ilmenite. High-Ti gabbro 2946. (d) Ilmenite crystal with lamellae and granules of titanomagnetite. Hornblendite, 3138 (cf. analyses 6, 7 in Table 2).

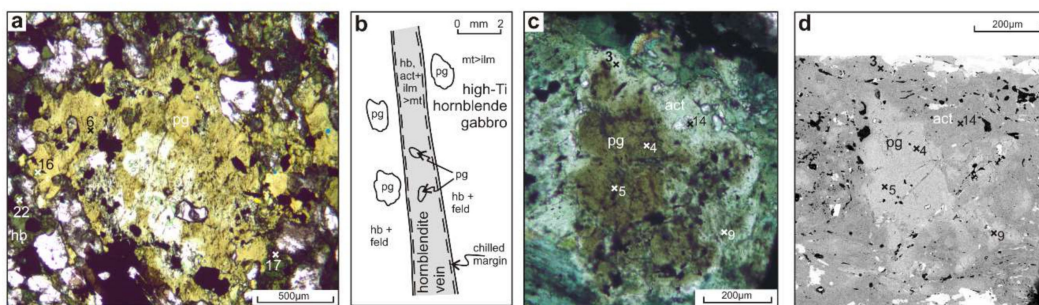


Figure 6. Petrographic microscope photomicrographs of amphiboles from a high-Ti hornblende gabbro (sample 3150). act: actinolite, feld: feldspar, hb: hornblende, ilm: ilmenite, mt: magnetite, pg: pargasite. (a) Ragged pargasite crystals (spots 16, 6) surrounded by small prisms of hornblende (spots 22, 17) [ppl]. (b) Schematic representation of the textural relationships between the high-Ti hornblende gabbro, hornblendite dyke and large pargasite crystals. (c) Large brown pargasite crystal in a hornblendite dyke (spots 4, 5, 9) with actinolite rims (spots 14, 3) [xpl]. (d) Back-scattered electron image of (c).

Table 2. Representative analyses of Fe–Ti oxides by electron microprobe.

Analysis Sample	Hornblendites							High-Ti Hornblende Gabbro				
	1 C2996 -3	2 C2996 -6	3 C2996 -5	4 C3138 -3	5 C3138 -9	6 C3138 -1	7 C3138 -1b	8 C3138 -6	10 C2969 -5	11 C2969 -2	12 C2969 -7	13 C2969 -6
SiO ₂	-	-	-	-	-	-	0.03	-	-	-	-	-
TiO ₂	0.2	45.59	0.4	0.19	49.16	42.62	3.62	3.01	0.14	45.7	0.35	48.8
Al ₂ O ₃	0.43	0.1	0.14	0.24	0.03	0.06	0.08	0.16	0.17	0.07	0.17	0.07
FeO _T	92.27	51.87	91.59	91.83	47.92	53.5	90.89	89.69	92.8	48.24	91.93	46.06
MnO	0.2	1.78	0.21	0.16	1.49	1.48	0.15	0.18	0.2	3.63	0.18	3.76
MgO	0.03	0.07	0.01	-	0.02	0.04	-	0.01	-	0.05	-	0.08
CaO	0.03	0.05	0.08	0.05	0.03	0.03	0.03	0.05	0.04	0.03	0.05	0.01
Na ₂ O	0.17	0.15	0.17	0.17	0.14	0.15	-	0.17	0.17	0.14	0.17	0.14
Cr ₂ O ₃	0.34	0.22	0.78	0.25	0.19	0.17	0.15	0.26	0.25	0.18	0.27	0.18
Total	93.67	99.83	93.38	92.89	98.98	98.05	94.95	93.53	93.77	98.04	93.12	99.1
Recalculated Analyses												
<i>Ilmenite-Hematite basis</i>												
Fe ₂ O ₃	14.13				5.81	18.54			12.06		6.75	
FeO	39.14				42.68	36.8			37.38		39.98	
Total	100.81				99.2	99.54			98.88		99.44	
Mol.%R ₂ O ₃	13.57				5.63	17.97			11.77		6.57	
<i>Magnetite-Ulvospinel basis</i>												
Fe ₂ O ₃	67.98		67.34	67.7			61.6	62.43	68.55			67.61
FeO	31.03		30.92	30.84			33.91	33.45	31.05			31.02
Total	99.87		99.02	99.13			99.47	99.24	100.1			99.33
Mol.%Usp	0.58		1.17	0.55			10.38	8.75				1.02
High-Ti Hornblende Gabbros												
Analysis Sample	14 C3150 -4	15 C3150 -12	16 C3150 -6	17 C3150 -5	18 C3150 -7	19 C3150 -8	23 C2947 -3	24 C2947 -10	25 C2947 -12	Pegmatitic Hornblendite		27 C3119 -2
SiO ₂	0.04	0.04	0.06	-	-	-	0.07	28.33	0.04			0.06
TiO ₂	0.07	48.9	0.08	49.7	0.71	48.7	49.91	37.31	48.58			0.03
Al ₂ O ₃	0.09	0.04	0.08	0.01	0.08	0.05	0.03	1.08	0.02			0.11
FeO _T	93.31	44.1	92.8	47.6	92.7	44.8	44.44	5.2	43.49			93.52
MnO	0.01	4.42	0.02	2.29	0.09	4.09	3.38	0.24	3.53			-
MgO	0.03	0.07	0.03	0.06	0.02	0.08	0.06	0.08	0.06			0.04
CaO	-	0.25	0.12	0.03	0.09	0.06	0.06	27.34	0.23			-
Na ₂ O	-	-	-	-	-	-	-	-	-			-
Cr ₂ O ₃	0.13	-	0.1	0.05	0.1	-	-	-	-			0.09
Total	93.68	97.8	93.2	99.8	93.8	97.8	97.95	99.56	95.94			93.85
Recalculated Analyses												
<i>Ilmenite-Hematite basis</i>												
Fe ₂ O ₃	5.12		5.93		5.82		3.31	3.8		7.02		
FeO	39.5		42.3		39.5		41.46	40.07		39.6		
Total	98		100		98.3		98.22	96.1		98.85		
Mol.%R ₂ O ₃	5.04		5.65				3.26	3.8		6.85		
<i>Magnetite-Ulvospinel basis</i>												
Fe ₂ O ₃	68.88		68.5	67.7								69.05
FeO	31.25		31.1	31.7								31.31
Total	100.4		99.9	100								100.6
Mol.%Usp	0.36		0.46	2.05								0.32

1, 2: independent crystals of magnetite and ilmenite; 3: inclusion in amphibole crystal; 4, 5: independent crystals of magnetite and ilmenite; 6: ilmenite crystal with magnetite lamellae (7) and granules (8); 10, 11: independent crystals of magnetite and ilmenite; 12, 13: composite crystals; 14, 15: independent crystals in the host gabbro; 16, 17: composite crystal in the host gabbro; 18, 19: independent crystals in amphibole veinlet; 22: independent crystal; 23: independent crystal; 24, 5: titanite crystal (24) with ilmenite patches (25) and lamellae; 26, 27: independent crystals.

5.3. Coupled Substitutions

The coupled substitutions in the pargasite–magnesianhornblende–actinolite series in the hornblende gabbros were examined in order to determine their principal substitutions. The element abundances expressed as total cations were examined first (Figure 3), as they are not affected by the distribution of elements to particular structural sites and assumptions on partitioning ferrous and ferric iron. Prominent changes in the vectors in the composition space are seen in Ti vs. Si and K vs. Si, both at Si ≈ 7.1 (Figure 3a,g). There is also a difference in Mg vs. Si between pargasite and other calcic amphiboles (Figure 3f). A few analyses from hornblendite and pegmatitic hornblendite show strong enrichment in Fe (and corresponding depletion in Mg) (Figure 3f,h,i).

For most amphiboles, there is only a narrow range of values of Mg/(Fe_T + Mg) so that, with the uncertainties in partitioning Fe, caution must be used in interpreting the variations in Mg. There is a strong negative correlation between Mg and ^{iv}Al for all of the amphiboles, with pargasite being the

least magnesian and actinolite being the most so (Figure 7a). Furthermore, individual zoned crystals of hornblende show an increase in $Mg/(Mg + Fe_T)$ from the core to the rim.

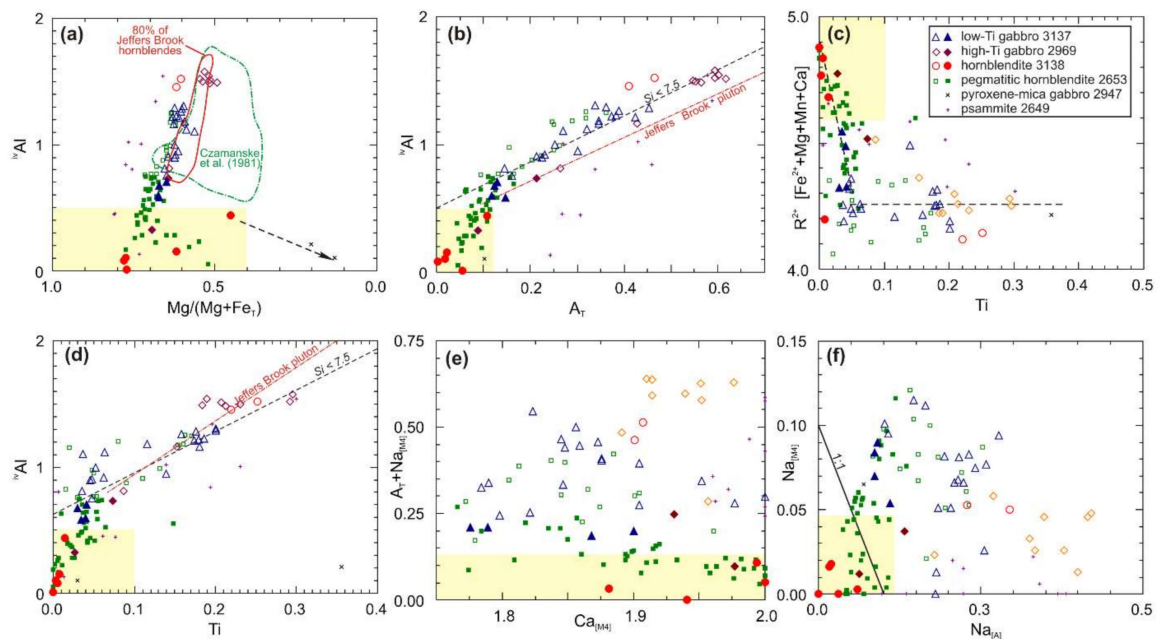


Figure 7. Plots showing the various element substitutions of the studied amphiboles. The field for the actinolite is shown in yellow. The atomic formulae were calculated on the basis of the mean of 13 and 15 cations in order to facilitate comparison with older data. (a) Plot of ${}^{iv}Al$ against $Mg/(Fe_T + Mg)$ showing the systematic change in Mg content from pargasite to actinolite. Note the increasing Fe in some actinolites. The Jeffers Brook pluton and Japanese plutons of Czamanske et al. [16] have lower $Mg/(Fe_T + Mg)$. (b) Plot of tetrahedral ${}^{iv}Al$ versus A site occupancy, to illustrate the edenite substitution. (c) Plot of R^{2+} against Ti, to illustrate the substitution $Ti R^{2+} = 2 {}^{vi}Al$. (d) Plot of ${}^{iv}Al$ against Ti, to illustrate the substitution $Ti + {}^{iv}Al = {}^{vi}Al + Si$. (e) Plot of $Na_{[M4]} + (Na + K)_{[A]}$ vs. $Ca_{[M4]}$ to illustrate the possible richterite substitution. Note the weak systematic trends for the different samples. (f) Plot of $Na_{[M4]}$ vs. $Na_{[A]}$, to illustrate the possible richterite substitution.

The edenite-type substitutions of the ${}^{iv}Al + (Na + K)_{[A]} = Si + A\text{-site vacancy}$ are illustrated in Figure 7b. As the Si decreases from magnesiohornblende to pargasite, the ${}^{iv}Al + (Na + K)_{[A]}$ steadily increases, with a 1:1 relation between the ${}^{iv}Al$ and $(Na + K)_{[A]}$, with an intercept at about 0.5 ${}^{iv}Al$ for 0.0 $(Na + K)_{[A]}$. The actinolites show a steeper trend with more scatter.

Richterite-type substitutions of the $Na_{[M4]} + (Na + K)_{[A]} = Ca_{[M4]} + A\text{-site vacancy}$ are shown in Figure 7e,f. A plot of $Na_{[M4]} + (Na + K)_{[A]}$ vs. $Ca_{[M4]}$ (Figure 7e) shows considerable scatter, but with weak inverse correlation within the individual samples implying some richterite substitution. In a plot of $Na_{[M4]}$ vs. $Na_{[A]}$ (Figure 7f), almost all of the analyses have greater $Na_{[A]}$ than $Na_{[M4]}$, and the individual rock samples show very scattered inverse trends, implying that the richterite substitution preferentially fills the A-site, particularly for low Si amphiboles like pargasite.

5.4. Geobarometry and Geothermometry Estimates

The physico-chemical conditions of the igneous calcic amphiboles can be estimated using equations proposed by Ridolfi et al. [13], which generally match the estimates from Anderson and Smith [17]. Macrocrystic pargasite, which appears to be xenocrystic or possibly phenocrystic in high-Ti gabbro, gives temperatures in the range of $890\text{--}900 \pm 25$ °C and pressures of $235\text{--}270 \pm 30$ MPa, equivalent to a mid-crustal depth of ~ 10 km. Magnesiohornblende in hornblende and both high- and low-Ti gabbro, with an igneous interlocking texture, yields temperatures of mostly $\sim 850 \pm 25$ °C and

pressures of $170\text{--}200 \pm 30$ MPa, equivalent to an upper crustal depth of ~ 7 km, but some actinolitic hornblende gives lower temperatures (>670 °C) and pressures (>30 MPa), implying depths of 1–2 km. Hornblendite pegmatites that cross-cut hornblende gabbros (Figure 6b) give temperatures of $820\text{--}710$ °C and pressures of ~ 45 MPa, suggesting an emplacement depth of only 2 km. The greater temperatures and pressures of the main hornblende gabbros may indicate that the principal crystallization in a crystal mush took place at ~ 7 km, but the final emplacement of that mush was at a much shallower depth. Rare actinolite rims of likely sub-solidus or hydrothermal origin in gabbros, with compositions suitable for temperature and pressure estimates, indicate temperatures of $670\text{--}690$ °C and pressures of 30–40 MPa. Metasomatic pargasite in psammite does not have compositions suitable for temperature and pressure estimates. The temperature values are reasonable, since the solidus for a gabbro–diorite melt at low pressures is >750 °C, rising to 850 °C at 0.9 GPa [18,19].

6. Results: Other Mineral Phases

6.1. Fe–Ti Oxides

The Fe–Ti oxides typically make up 1 to 2% of the mafic rocks, occurring principally as late stage anhedral grains, but also as fine-grained inclusions in primary biotite and amphibole. Rarely, they occur as coarse- to medium-grained overgrowths on ferromagnesian minerals. The dominant oxide mineral is ilmenite (Table 2); magnetite also occurs in some samples. Titanomagnetite was not identified in any sample, except as exsolution lamellae and granules in ilmenite in a hornblendite (analyses 7, 8 in Table 2; Figure 5d).

Ilmenite is the only oxide mineral in the pegmatitic hornblendite, the pyroxene–mica gabbro, and some other hornblende gabbros, where it is predominantly interstitial. It has a variable but substantial MnO content (1.5–4.5%). The MnO content is highest in the pyroxene–mica gabbro, the high-titanium hornblende gabbros, and the pegmatitic hornblendite, which may indicate that these rocks crystallised under conditions of higher oxygen fugacity than the other gabbros [20]. In individual crystals, the MnO content is either uniform or increases towards the margins of the crystals, which suggests a gradual increase in oxygen fugacity. There is no detectable Mn and very low amounts of Ti in the magnetites (Table 2).

In the pyroxene–mica gabbro, some opaque crystals have outlines similar to those of titanite, and some have a bulk chemical composition similar to titanite (e.g., analysis 24 in Table 2). These same crystals contain ilmenite lamellae (analysis 25 in Table 2) and ilmenite patches, apatite inclusions, and biotite–chlorite patches (Figure 5b). The opaque colour of these titanite crystals is due to the presence of ilmenite. These opaque titanite crystals presumably represent early crystallised titanite. The partial replacement of titanite by ilmenite (Figure 5b) is likely associated with the chloritization of biotite and the sericitization of plagioclase, and it must have taken place under reducing conditions, as the formation of ilmenite should involve Fe^{2+} [21].

The interstitial ilmenite in some hornblendites contains tiny lamellae and drop-like bodies of magnetite (Figure 5d; analyses 7, 8 in Table 2). In the same sample, magnetite tends to be concentrated in a reaction zone between actinolite with a clinopyroxene crystal habit, presumably pseudomorphing clinopyroxene, poikilitically enclosed by hornblende (Figure 5a). Similar textures have been described from the Finnmarka Complex in Norway [20], and ascribed to the reduction of the Fe_2O_3 component of the ilmenite–hematite solid solution series during cooling in a closed water-bearing system, perhaps within crystals that have a greater Fe_2O_3 component in their cores. A similar explanation is suggested for the ilmenite host of Figure 5d that also has a high Fe_2O_3 component (Table 2, analysis 6). In addition, parallel rod-like bodies of ilmenite occur in both the actinolite and the hornblende (Figure 5a).

Composite crystals of ilmenite and minor magnetite are common in both hornblende gabbros and hornblendites. Such composite grains suggest that the original grain comprised an ulvospinel component that subsequently unmixed by oxidation to ilmenite and magnetite [22]. On the other hand,

both ilmenite and magnetite may have formed directly from a titanomagnetite grain by oxidation [20]. In sample 3150 (Figure 6), individual crystals of magnetite and ilmenite occur both in the dyke (in which ilmenite predominates) and within the host gabbro (in which magnetite predominates). This may indicate a return to reducing conditions during formation of the dyke.

Most of the opaque inclusions in the amphiboles and biotites that were analysed consist of ilmenite, which occurs in pargasite (sample 3150), hornblende (2947, 3150) and actinolite (3138). Magnetite inclusions in the amphiboles were seen only in the hornblendite sample (3138) described above.

Some of the minor felsic rocks contain no Fe–Ti oxides, and where they are present they make up less than 0.5% of the rock. The Fe–Ti oxides consist of independent crystals of either ilmenite or magnetite, or composite crystals of these two minerals with magnetite predominating. The magnetite contains a high hematite and a low ulvospinel component. The low ulvospinel content of the magnetites reflects the unusually-high oxygen fugacity, or the unusually-low equilibration temperature, or both [20]. The trend from ilmenite in less-silicic to magnetite in more-silicic rocks has been ascribed to the progressive oxidation in the more-silicic rocks [20].

In summary, ilmenite is an early mineral in most rock types, and it continued to form throughout the crystallisation of the rocks. It is most common in the high-Ti gabbro, pyroxene–mica gabbro and hornblendite dykes. Magnetite is locally developed in some clinopyroxene cores, and some early hornblendite and is also predominant in felsic rocks. A variety of sub-solidus textures reflect the exsolution of oxide phases as cooling took place. The chemical composition of magnetite does not vary significantly between the different rock types, but ilmenite has a higher hematite content and a lesser abundance of TiO₂ and MnO in most hornblendites.

6.2. Pyroxenes

The clinopyroxene in the low-Ti hornblende gabbros is predominantly salite (augite). The orthopyroxene of the hornblendite is ferro-hypersthene, with a composition of about En₄₀ Fs₆₀ (Table 3).

The clinopyroxene from the pyroxene–mica gabbro, although also salite, is distinct, with high Ti and a low Mg/(Mg + Fe) ratio, showing strongly-alkaline chemistry, whereas clinopyroxenes from the other gabbros are alkaline–subalkaline [23].

6.3. Biotite

Biotite is a texturally late, minor constituent which occurs as a replacement of amphibole or interstitial to most rock-forming minerals. It has also been found as inclusions in titanite (Figure 5b) in the pyroxene–mica gabbro. Representative biotite analyses from a range of rock types (Table 4) show no systematic changes in the unit cell content of K between hornblende gabbros and granitic pegmatites. The Mn and ^{vi}Al are lower in biotites in gabbro than those in granitic pegmatite, which are also of quite different chemistry from those in the nearby McCallum Settlement granite plutons.

The contents of TiO₂, FeO_t, MgO and Mg/Mg + Fe in biotites tend to be high in the high-Ti hornblende gabbros, correlating in general with the whole rock chemistry. The ^{vi}Al in the biotites is variable in these rocks: this variation is probably related to the temperature of its formation [25], with the pyroxene–mica gabbro crystallising at the highest temperature. Some of the biotite in the pyroxene–mica gabbro has been—in part—altered to chlorite, which includes lamellae of titanite (Figure 5c) with small patches of ilmenite. The fresh biotite in the rock has unusually high iron and titanium: the development of the titanite and ilmenite thus appears to be the result of oxidation.

Table 3. Representative analyses of the pyroxenes by electron microprobe.

Analysis	Hornblende				Px-Mica Gabbro		Psammite ⁺	
	1	2	3	4	5	6	7	9
Sample	C2996	C2996	C2996	C3138	C3138	C2947	C2947	C2648A
Mineral	Opx	Opx	Cpx	Cpx	Cpx	Cpx core	Cpx rim	Cpx
Location								
SiO ₂	52.85	56.01	52.4	51.76	52.59	47.21	47.59	53.39
TiO ₂	0.16	0.04	0.28	0.36	0.23	2.91	2.13	
Al ₂ O ₃	1.46	0.34	1.89	2.26	1.71	5.38	4.49	1.09
FeO _t	23.85	20.82	8.89	8.94	8	11.89	12.36	5.2
MnO	0.77	1.04	0.35	0.41	0.38	0.34	0.36	0.24
MgO	20.99	19.63	13.68	13.26	13.46	10.38	10.51	16.07
CaO	0.49	1.02	22.79	22.7	24.09	21.28	20.38	24.64
Na ₂ O	0.04	0.07	0.39	0.38	0.35	0.69	0.68	0.09
K ₂ O	-	-	-	-	-	0.04	0.04	0.04
Cr ₂ O ₃	0.08	0.04	0.08	0.06	0.07	0.08	0.11	0.08
Total	100.69	99.01	100.75	100.13	100.89	100.2	98.65	101.12
Structural formulae on the basis of 6 Oxygen atoms								
Si	1.971	2.129	1.937	1.98	1.941	1.787	1.829	1.94
Al ^{IV}	0.029	0.129	0.063	0.072	0.059	0.213	0.171	0.047
Al ^{VI}	0.036	0.144	0.02	0.027	0.015	0.027	0.032	-
Ti	0.004	0.001	0.008	0.1	0.006	0.083	0.062	0.008
Fe ³⁺ *	-	-	0.053	0.05	0.055	0.071	0.065	0.063
Fe ²⁺	0.744	0.662	0.222	0.228	0.192	0.305	0.332	0.095
Mn	0.024	0.033	0.011	0.013	0.012	0.002	0.012	0.007
Mg	1.167	1.112	0.754	0.736	0.74	0.585	0.602	0.87
Ca	0.02	0.042	0.903	0.906	0.953	0.863	0.839	0.959
Na	0.003	0.005	0.028	0.027	0.025	0.051	0.051	0.006
K	-	-	-	-	-	0.002	0.002	0.002
Cr	0.002	0.001	0.002	0.002	0.002	0.002	0.003	0.002
100 Mg/ Mg + Fe	61.07	62.68	73.27	72.58	74.97	60.87	60.02	84.63

⁺ Thermally-metamorphosed at the margin of the pluton. * For the recalculation of the total iron to Fe³⁺ and Fe²⁺, the method of [24] was used.

Table 4. Representative analyses of biotite by electron microprobe.

Analysis	Hornblende	Hi-Ti Hornblende Gabbros	Px-Mica Gabbro			Granite	Granite
	1	2	3	4	5	6	7
Sample	C2996	C3150	C3150	C2946	C2947	C2984	C3136
SiO ₂	36.58	36.45	36.17	35.31	35.93	35.1	35.76
TiO ₂	2.96	2.41	2.57	3.55	4.62	2.74	2.5
Al ₂ O ₃	15.94	15.86	15.97	14.72	13.54	17.65	16.35
FeO _t	18.29	19.27	20.38	25.67	26.43	23.23	18.52
MnO	0.14	0.19	0.23	0.16	0.21	0.63	0.31
MgO	12.11	11.53	10.79	7.41	6.58	7.41	11.27
CaO	-	0.05	0.07	0.08	0.08	0.04	0.1
Na ₂ O	0.22	-	0.11	0.04	0.16	0.05	0.11
K ₂ O	9.21	9.88	9.63	9.66	9.69	9.27	9.37
Total	95.45	95.64	95.92	96.6	97.24	96.12	94.29
Structural formulae on the basis of 22 Oxygen atoms							
Si	5.531	5.546	5.522	5.504	5.588	5.41	5.498
Al ^{IV}	2.469	2.454	2.478	2.496	2.412	2.59	2.502
Al ^{VI}	0.371	0.391	0.472	0.208	0.069	0.615	0.461
Ti	0.334	0.275	0.244	0.416	0.539	0.317	0.288
Fe	2.312	2.453	2.4	3.346	3.439	2.994	2.383
Mn	0.015	0.024	0.018	0.02	0.026	0.081	0.04
Mg	2.73	2.616	2.671	1.72	1.525	1.701	2.581
Ca	-	0.007	0.018	0.013	0.011	0.004	0.015
Na	0.064	-	0.024	0.011	0.046	0.013	0.033
K	1.777	1.918	1.789	1.921	1.925	1.824	1.839
100 Mg/(Mg + Fe)	54.15	51.61	52.67	33.96	30.72	36.22	50.89
(MgO/FeO) _{rock}	0.68	0.38	0.38	0.32	0.36	0.48	1.77

6.4. Feldspar

Plagioclase feldspar is present in all of the rocks studied; K-feldspar occurs in the pyroxene–mica gabbro and the felsic rocks. Plagioclase compositions in the hornblendite range from bytownite to labradorite, and in the hornblende gabbro range from labradorite to andesine. Albite is present in the pyroxene–mica gabbro, where coarse albite and K-feldspar crystals interlock; in such a mafic rock, the albite is presumably an alteration product, and the K-feldspar compositions are unlikely to be magmatic. Some hornblendite and hornblende gabbro contain albitic patches in plagioclase and some interstitial K-feldspar. The high-Ti hornblende gabbro sample 2969 has labradorite crystals with patchily-altered cores of Na-rich feldspar composition. In all of the rocks, the larger plagioclase crystals show multiple twinning and oscillatory zoning, whereas the smaller crystals show normal zoning to more sodic compositions towards the rim. In the felsic rocks, K-feldspar may be rimmed by andesine with albitic patches.

6.5. Sulphides and Carbonates

Minor amounts (<0.2%) of sulphides and carbonates are present in most of the studied samples. Pyrite, chalcopyrite, bornite, siderite and calcite were identified in the electron microprobe studies. Pyrite usually occurs as inclusions within ferromagnesian minerals, and—in this association—is generally accompanied by chalcopyrite and siderite, forming composite grains. The textures of these composite grains suggests that the siderite formed after the sulphide minerals. Pyrite also occurs in association with Fe–Ti oxides, and—in this association—moulds itself upon these minerals. Pyrite, chalcopyrite and siderite occasionally form interstitially. The textures of the sulphides and siderite likely represent hydrothermal alteration along hairline fractures, despite their occurrence within amphiboles, biotite and orthopyroxene.

7. Discussion

7.1. Coupled Substitutions in Amphiboles

The coupled substitutions in the pargasite–magnesiohornblende–actinolite series in the hornblende gabbros were compared with data from the coeval Jeffers Brook tonalite–granodiorite pluton [9], and with literature data from calc-alkaline granodiorites [16,26,27] and ultramafic rocks [28]. Two significant changes in the exchange vectors have been identified. In the edenite substitution, the ${}^{\text{iv}}\text{Al}$ vs. $(\text{Na} + \text{K})_{[\text{A}]}$ vector changes from magnesiohornblende to actinolite because no K is present in the actinolite structure. The Ti substitution in the actinolite takes place through $\text{Ti} \text{R}^{2+} = 2 \text{}^{\text{vi}}\text{Al}$, whereas in magnesiohornblende and pargasite the dominant substitution appears to be $\text{Ti} + \text{}^{\text{iv}}\text{Al} = \text{}^{\text{vi}}\text{Al} + \text{Si}$.

The most significant chemical differences between the Frog Lake pluton amphiboles and those in more felsic calc-alkaline plutons [16,26,27], including the Jeffers Brook pluton [9], relate to the abundance of Fe (Figure 7a), with the $\text{Mg}/(\text{Mg} + \text{Fe}^{2+})$ generally being lower in the Frog Lake amphiboles. This may be, however, an artefact of the higher ${}^{\text{iv}}\text{Al}$ in the Frog Lake amphiboles, reflecting a greater depth of crystallisation [17]. The observed zoning in the amphiboles with an increase in $\text{Mg}/(\text{Mg} + \text{Fe}_{\text{T}})$ from the core to the rim has been interpreted to reflect the increasing oxygen fugacity as the magma became more siliceous [27–29]. Small differences are seen between the Frog Lake and Jeffers Brook plutons in other elements (e.g., Figure 7d), but no systematic pattern with the rock type has been detected. The decrease in the elements Na and K, with increasing Si (Figure 3d,g), suggests that these elements may be partitioned into a coexisting hydrothermal fluid phase that results from the devolatilisation of rising magma [26]. The similar decrease in Ti and Fe (Figure 3a,i) suggests that these elements may also be transported by hydrothermal fluids.

The inflection in the Ti abundance vs. Si (Figure 3a) appears to be related to changes in the dominant substitution involving Ti. At low Ti contents in actinolite, the correlation of Ti with R^{2+} sites suggests the predominance of the substitution $\text{Ti} \text{R}^{2+} = 2 \text{}^{\text{vi}}\text{Al}$ (Figure 7c), whereas in magnesiohornblende and

pargasite, the R^{2+} remains unchanged with increasing Ti. In these Si-poor minerals, the dominant substitution appears to be $Ti + {}^{iv}Al = {}^{vi}Al + Si$, based on the correlation of Ti with ${}^{iv}Al$ (Figure 7d). A similar trend has been reported from other calc-alkaline intrusions [9,16,26].

The trends of edenite-type substitutions (Figure 7b), with a distinctly different vector for actinolites, are found in calc-alkaline intrusions elsewhere [16,26,27]. The change in the vector is entirely due to the virtual absence of K in actinolite (Figure 3g). Samples from the Jeffers Brook pluton show rather higher values of $(Na + K)_{[A]}$ for any given ${}^{iv}Al$ value [9].

7.2. Magmatic and Hydrothermal Minerals

The principal minerals in the hornblende gabbro are clearly of magmatic origin, and form a crystallisation sequence from pargasite to magnesiohornblende to actinolitic hornblende, with corresponding changes in chemical composition (Figures 2, 3 and 7) and optical properties (Figures 4 and 6). The hornblende crystals have cores of pyroxene, which in many cases are pseudomorphed by sub-solidus actinolite. The magnesiohornblende crystals have rims of actinolitic hornblende and, exceptionally, actinolite. The actinolitic hornblende is considered to be a magmatic amphibole on the basis of its texture. The textural evidence is that much of the actinolite developed under sub-solidus conditions, but where actinolite rims are in optical continuity with pargasite or hornblende crystals, it suggests a continuous (but lower temperature) magmatic origin, rather than a secondary origin. The presence of an actinolite rim on pargasite phenocrysts, in a dyke with a chilled margin, is further evidence for a primary igneous origin for this actinolite (Figure 6b,c).

Some other minerals are clearly of hydrothermal origin. These include sulphides such as pyrite and chalcopyrite, and carbonates such as siderite and calcite that developed along fractures in ferromagnesian minerals. Albite occurs in patches in some plagioclase, and albite + quartz forms the cores of some amphibole phenocrysts, probably replacing original plagioclase.

7.3. Conditions of the Crystallisation of Magmatic Minerals

Compositional clusters in the lower-Si amphiboles (pargasite and magnesiohornblende), together with changes in colour, suggest that the amphibole crystallisation was episodic, not continuous. This most likely reflects the episodic rise of magma and/or release of volatiles, with the pargasite cores forming at the greatest depths in the rising magma column.

The available mineralogical data suggest changes in the oxygen fugacity from early to late magmatic conditions, and then during the sub-solidus recrystallisation. The presence of magnetite in pseudomorphs after clinopyroxene cores, and in some early hornblendites, suggests somewhat-oxidising conditions. The dominance of ilmenite in most of the gabbros and hornblendites indicates that the main crystallisation of the magma took place under reducing conditions. The increase of Mn towards the margin of the ilmenite crystals is taken to indicate the gradual increase of oxygen fugacity, and thus the establishment of more oxidising conditions. The precipitation of titanite in almost all of the studied samples, and the presence of ferrohypersthene in the hornblendites are also evidence that the oxygen fugacity was high during the later stages of the crystallisation [20]. The replacement of titanite by ilmenite and other silicate minerals, the lamellae of titanomagnetite in the ilmenite, and the ilmenite lamellae in the amphiboles (Figure 5) all suggest subsequent reducing conditions, probably in the early stages of the sub-solidus crystallisation. The metasomatism seen in the pyroxene–mica gabbro is also likely a sub-solidus process. The almost complete lack of Ti in the magnetite (Table 2) implies that the cooling of the pluton was slow [30].

The extensive development of titanite in some pegmatitic hornblendites near the contact with the country rock, both as inclusions in amphibole crystals and as large independent crystals, and its occurrence in felsic pegmatites suggests that the magmatic titanite formed during the later stages of the crystallization of the Frog Lake pluton. These titanite crystals may also have retained the TiO_2 and incompatible trace elements which are highly depleted at the margin of the psammite [4]. Such titanite is an indicator of a highly oxidising environment. The dominance of magnetite in the minor granites

of the Frog Lake pluton also indicates oxidising conditions. The titanite crystals were subsequently affected by the subsolidus hydrothermal alteration producing pseudomorphs after titanite that contain ilmenite and very fine grains of other minerals, as has been noted elsewhere [21].

The significance of the pegmatitic textures in the hornblende is unclear, beyond the crystallisation of amphibole requiring a hydrous magmas. Hornblende–plagioclase pegmatites have been reported from a wide range of crustal depths [31,32]. The interpretation has generally paralleled the interpretation of better known granitic pegmatites, which are commonly interpreted as resulting from the presence of free water [33] or from the depolymerisation of highly hydrous magmas [34,35]. However, fluid inclusion studies of an Archean hornblende pegmatite show that it crystallised in the presence of a carbonic fluid [36]. Recent work has shown that granitic pegmatites result not from free water, but from particular conditions of undercooling and the rapid growth rates of crystals [37], and it is likely that an analogous process might have been responsible for hornblende pegmatite.

7.4. Evolution of Fluids during the Crystallisation of Calc-Alkaline Plutons

A comparison of the mineralogy of rocks of similar chemical composition from the Jeffers Brook and Frog Lake plutons, which are interpreted to represent different structural levels, may provide insight into the roles of rising hydrothermal fluids on minerals within a cooling calc-alkaline subduction-related system (Table 5).

The geophysical data show that, in modern subduction zones, intergranular super-hydrous (>8 wt% dissolved H₂O) partial melts of andesite tend to pond at mid-crustal depths (15–20 km, 600 MPa) [38]. Magmas and crystal mushes that rise further through the crust crystallise and devolatilise as they ascend [39,40], providing abundant hydrothermal fluids within a complex magma conduit.

Field and textural observations within the two plutons suggest the different behaviours of their magmas are probably a result of the different structural levels. The Frog Lake pluton, at a deeper structural level, appears to have been a pathway for multiple magma batches in an actively deforming and widening strike-slip fault system. At least some of the larger bodies are sills [4]. It has common pegmatitic dykes with large hornblende crystals. It also has common tonalite dykes showing syn-magmatic deformation along with the gabbro. Also present are irregular segregations or enclaves of granitic composition that may represent patches of immiscible felsic magma [41]. The Jeffers Brook pluton is a compositionally-differentiated laccolith at a shallow depth that appears to involve fewer magma emplacement events, with mafic magmas forming pods with chilled margins and mafic microgranular enclaves within the main tonalite–granodiorite [5].

The amphiboles in the hornblende gabbros of the Jeffers Brook pluton [9] show many similarities to those of the Frog Lake pluton (Table 5). In both plutons, actinolite appears to pseudomorph clinopyroxene, and to develop at the expense of hornblende. The pargasite in the Jeffers Brook pluton and in the Frog Lake pluton may be found as cores to hornblende. The actinolitic hornblende occurs as rims in optical continuity with magnesiohornblende, and is therefore of igneous origin.

The composition of the magnesiohornblende in the Jeffers Brook pluton [9] is less aluminous than that of the Frog Lake pluton (Figure 7b), a variation that in a similar magma type is principally related to lower pressure [17]. The more Mg-rich cores in some amphiboles of the Jeffers Brook pluton probably reflect a greater original depth of crystallisation in a mid-crustal magma chamber prior to the emplacement.

The actinolitic hornblende rims are more prominently developed in the Frog Lake pluton than in the Jeffers Brook pluton. This may be a consequence of the higher temperatures and lower oxygen fugacity in the Frog Lake pluton, resulting from the higher proportion of mafic magma. Experimental investigations [42] demonstrated the high thermal stability of actinolite with Fe-numbers of 0–0.4, which is the case for the analyses of the actinolite in Figure 6c, at temperatures of 750–900 °C. They thus overlap the range of water-saturated melting for a typical andesite or tonalite. Patchy Mg-rich compositional domains that are indicative of high oxygen fugacity, which have been interpreted [26] as

a subsolidus product, are much less common in the Frog Lake amphiboles compared with the Jeffers Brook amphiboles, where temperatures were lower.

Magnetite is the principal iron–titanium oxide in the Jeffers Brook pluton, compared with ilmenite (reflecting a lower oxygen fugacity) in the Frog Lake pluton. In both plutons, most early amphiboles crystallised under conditions of low oxygen fugacity, indicated by the low Mg content of the amphiboles. However, the presence of magnetite in some pseudomorphed clinopyroxene cores and early hornblende may indicate an early, more oxidising stage.

Many of these differences between the two plutons appear to be related to variations in the behaviour of the hydrous components. In the Frog Lake pluton, the crystallisation of the amphibole removed water from the mafic magma, so that the gabbroic magma was less oxidizing, and subsolidus processes did not take place in the presence of abundant water. Any felsic magma remained strongly hydrous, and thus the felsic rocks show evidence of the most extreme oxidation. The Jeffers Brook laccolith was water-saturated, as it trapped hydrothermal waters resulting from devolatilisation of rising magmas in the underlying magma column.

Table 5. Summary of the differences between the Frog Lake and Jeffers Brook plutons.

<i>General Geology</i>	Frog Lake Pluton	Jeffers Brook Pluton
Age	~622 Ma	~606 Ma
Outcrop dimensions	4 km ²	3 km ²
Country rock	medium-grade Mesoproterozoic Gamble Brook Fm. quartzite and metapelite	low-grade Neoproterozoic Jeffers Group volcanic and volcanoclastic rocks
Style of intrusion	vertical sheets within country rock	laccolith, underlying sills
Predominant rock type	hornblende gabbro	tonalite and granodiorite
Important minor rock types	hornblende, tonalite, mafic and felsic pegmatites	diorite pods and enclaves, granite and aplite dykes, gabbro sills and enclaves
Irregular felsic patches	common	rare
<i>Mineral composition of mafic rocks</i>		
Magmatic amphiboles	pargasite, hornblende, actinolitic hornblende, minor actinolite	pargasite, hornblende, minor actinolitic hornblende
Subsolidus amphiboles	actinolite, some Fe-rich	actinolite, some Mg-rich
Amphibole chemistry	generally similar, but ^{IV} Al higher	generally similar, but ^{IV} Al lower
Fe-Ti oxides	ilmenite predominant, but late magmatic magnetite	magnetite predominant, but common early ilmenite
Subsolidus exsolution textures of Fe-Ti oxides	Ti-magnetite exsolution in ilmenite; exsolution of ilmenite in hornblende and actinolite; replacement of titanite by ilmenite	not seen
<i>Physical and chemical properties of magmas</i>		
Inferred oxygen fugacity	Moderate in early crystals, becoming low as Hbl crystallized	Moderate in early crystals, becoming high as main rocks crystallized.
Ridolfi et al. (2010) amphibole geothermometry and geobarometry	900–670 °C, 270–30 MPa; hornblende pegmatite 820–710 °C, ~45 MPa.	950–670 °C, 300–25 MPa
Behaviour of hydrous components	Mafic magma undersaturated in H ₂ O due to crystallisation of amphibole; felsic magma saturated.	At least the tonalite-granodiorite magma water saturated by trapped rising hydrothermal fluids.

Another key difference between the two plutons is that the Frog Lake pluton appears to have been formed by many small magma batches that progressively filled the widening shear zone as a series of dykes (Figure 1f). These batches acted as closed systems, so that as hornblende crystallised, the dissolved water content of the magma was reduced, despite the reduced solubility of water in rising magma. Thus, the earliest phases may have crystallised under more oxidising conditions, but the main crystallisation of the hornblende was under more reducing conditions. Under sub-solidus conditions, the buffering effect of the amphibole crystallisation was no longer active, so that the residual felsic magmas accumulated water and were more oxidising. Rising hydrothermal fluids from the devolatilisation of deeper rising magmas resulted in hydrothermal alteration under more oxidising conditions. In the Jeffers Brook pluton, there is no evidence for nearly as many mafic magma batches, and the dominant tonalite–granodiorite had a much lower proportion of hydrous ferromagnesian minerals capable of buffering the water content of the magma. The genesis of the separate mafic and intermediate magma batches to both plutons took place deeper in the crust or mantle [4]. The Frog

Lake pluton or magma conduit probably was supplied with more mafic magma than that which was able to reach the higher level Jeffers Brook pluton.

8. Conclusions

1. The presence of multiple dykes in the mafic lithologies of the Frog Lake pluton, in a progressively widening shear zone, indicates that multiple small mafic magma batches were responsible for the construction of the Frog Lake pluton. These small magma batches favoured the reduction of water content by the crystallisation of hydrous ferromagnesian minerals and the trapping of minor felsic magma.
2. Some magma batches started to crystallise at a moderate oxygen fugacity, as indicated by the magnetite in some clinopyroxene cores and early hornblendites, but the main crystallisation of the amphiboles reduced the water saturation and took place under low oxygen fugacity. The magmatic amphiboles form a punctuated crystallisation sequence from pargasite to magnesiohornblende to actinolitic hornblende, with corresponding changes in chemical composition and optical properties. As the crystallisation came to its completion, the continuing supply of water from deeper devolatilising magma led to an increase in the oxygen fugacity in the residual felsic magma, and resulted in the precipitation of euhedral titanite crystals in the hornblendites and felsic pegmatites. The cooling of the Frog Lake pluton was slow, as indicated by the chemical composition of the magnetite, with almost no Ti, and is consistent with its mode of construction.
3. The decrease in elements such as Na, K, Ti and Fe in the analysed amphiboles suggests that there might have been some partitioning of these elements in a coexisting fluid phase that then produced the observed hydrothermal alteration, including the formation of albite and chlorite.
4. The comparison of the Frog Lake pluton with the coeval Jeffers Brook pluton, which was emplaced at a higher structural level based on its geological criteria, shows that the Jeffers Brook pluton crystallised at a higher oxygen fugacity. Thus, even for plutons broadly of the same chemical composition and same tectonic environment, other factors such as the structural level of the emplacement, the size and number of the magma batches, and the temperature and pressure conditions of the crystallisation influence their mineralogical evolution. These factors are dependent on the detailed structure of the particular pluton, and will affect their detailed mineralogy and petrology, and their potential to generate hydrothermal fluids.

Funding: This research was funded by Natural Sciences and Engineering Research Council of Canada (NSERC) discovery grants to G. Pe-Piper, most recently grant no. 2016-04310.

Acknowledgments: I thank David Piper for discussions, and Justin Nagle for help in preparing the manuscript.

Conflicts of Interest: The author declares no conflict of interest.

References

1. Mark, G.; Foster, D.R.W. Magmatic-hydrothermal albite-actinolite-apatite-rich rocks from the Cloncurry district, NW Queensland, Australia. *Lithos* **2000**, *51*, 223–245. [[CrossRef](#)]
2. Keppie, J.D.; Dallmeyer, R.D.; Murphy, J.B. Tectonic implications of $^{40}\text{Ar}/^{39}\text{Ar}$ hornblende ages from late Proterozoic–Cambrian plutons in the Avalon composite terrane, Nova Scotia, Canada. *Geol. Soc. Am. Bull.* **1990**, *102*, 516–528. [[CrossRef](#)]
3. Pe-Piper, G.; Piper, D.J.W. 1: 50,000 Geological Maps of the Cobequid Highlands. *Nova Scotia Department of Natural Resources*. 2005; Open File Map ME 2005-116 and Open File Map ME 2005-117.
4. Pe-Piper, G.; Piper, D.J.W.; Tsikouras, B. The late Neoproterozoic Frog Lake hornblende gabbro pluton, Avalon Terrane of Nova Scotia: Evidence for the origins of appinites. *Can. J. Earth Sci.* **2010**, *47*, 103–120. [[CrossRef](#)]
5. Pe-Piper, G.; Piper, D.J.W. The Jeffers Brook diorite–granodiorite pluton: Style of emplacement and role of volatiles at various crustal levels in Avalonian appinites, Canadian Appalachians. *Int. J. Earth Sci.* **2018**, *107*, 863–883. [[CrossRef](#)]

6. Murphy, J.B.; Blais, S.A.; Tubrett, M.; McNeil, D.; Middleton, M. Microchemistry of amphiboles near the roof of a mafic magma chamber: Insights into high level melt evolution. *Lithos* **2012**, *148*, 162–175. [[CrossRef](#)]
7. Murphy, J.B.; Hynes, A.J.; Cousens, B. Tectonic influence on late Proterozoic Avalonian magmatism: An example from the Greendale Complex, Antigonish Highlands, Nova Scotia, Canada. In *The Nature of Magmatism in the Appalachian Orogen: Geological Survey of America Memoir*; Sinha, A.K., Whalen, J.B., Hogan, J.P., Eds.; Geological Society of America: Boulder, CO, USA, 1997; Volume 191, pp. 255–274. ISBN 9780813711911.
8. Murphy, J.B.; Pe-Piper, G.; Piper, D.J.W.; Nance, R.D.; Doig, R. Geology of the Eastern Cobequid Highlands. *Geol. Surv. Can. Bull.* **2001**, *556*, 1–61.
9. Pe-Piper, G. The calcic amphiboles of mafic rocks of the Jeffers Brook plutonic complex, Nova Scotia, Canada. *Am. Mineral.* **1988**, *73*, 993–1006.
10. Doig, R.; Murphy, J.B.; Nance, R.D. U-Pb geochronology of Late Proterozoic rocks of the eastern Cobequid Highlands, Avalon Composite Terrane, Nova Scotia. *Can. J. Earth Sci.* **1991**, *28*, 504–511. [[CrossRef](#)]
11. Pe-Piper, G.; Piper, D.J.W.; Koukouvelas, I. The Precambrian plutons of the Cobequid Highlands, Nova Scotia. In *Avalonian and Related Peri-Gondwanan Terranes of the Circum-North Atlantic*; Special Paper 304; Nance, R.D., Thompson, M.D., Eds.; Geological Society of America: Boulder, CO, USA, 1996; pp. 121–132.
12. Schumacher, J.C. Appendix 2: The estimation of ferric iron in electron microprobe analysis of amphiboles. *Mineral. Mag.* **1997**, *61*, 312–321.
13. Ridolfi, F.; Renzulli, A.; Puerini, M. Stability and chemical equilibrium of amphibole in calc-alkaline magmas: An overview, new thermobarometric formulations and application to subduction-related volcanoes. *Contrib. Mineral. Petrol.* **2010**, *160*, 45–66. [[CrossRef](#)]
14. Leake, B.E.; Wooley, A.R.; Arps, C.E.S.; Birch, W.D.; Gilbert, M.C.; Grice, J.D.; Hawthorne, F.C.; Kato, A.; Kisch, H.J.; Krivovichev, V.G.; et al. Nomenclature of amphiboles: Report of the subcommittee on amphiboles of the International Mineralogical Association, Commission on New Minerals and Mineral Names. *Can. Mineral.* **1997**, *35*, 219–233.
15. Leake, B.E. Nomenclature of amphiboles. *Mineral. Mag.* **1978**, *42*, 533–563. [[CrossRef](#)]
16. Czamanske, G.K.; Ishihara, S.; Atkin, S.A. Chemistry of rock forming minerals of the Cretaceous–Paleogene batholith in southwestern Japan and implications for magma genesis. *J. Geophys. Res.* **1981**, *86*, 10431–10469. [[CrossRef](#)]
17. Anderson, J.L.; Smith, J.L. The effects of temperature and fO₂ on the Al-in-hornblende barometer. *Am. Mineral.* **1995**, *80*, 549–559. [[CrossRef](#)]
18. Wyllie, P.J.; Wolf, M.B. Amphibolite dehydration-melting: Sorting out the solidus. *Geol. Soc. London Spec. Publ.* **1993**, *76*, 405–416. [[CrossRef](#)]
19. López, S.; Castro, A. Determination of the fluid-absent solidus and supersolidus phase relationships of MORB-derived amphibolites in the range 4–14 kbar. *Am. Mineral.* **2001**, *86*, 1396–1403. [[CrossRef](#)]
20. Czamanske, G.K.; Mihalik, P. Oxidation during magmatic differentiation: Finnmarka Complex, Oslo area, Norway: Part 1, The Opaque Oxides. *J. Petrol.* **1972**, *13*, 493–509. [[CrossRef](#)]
21. Broska, I.; Harlov, D.; Tropper, P.; Siman, P. Formation of magmatic titanite and titanite-ilmenite phase relations during granite alteration in the Tribec Mountains, Western Carpathians, Slovakia. *Lithos* **2007**, *95*, 58–71. [[CrossRef](#)]
22. Buddington, A.F.; Lindsley, D.H. Iron-titanium oxide minerals and synthetic equivalents. *J. Petrol.* **1964**, *5*, 310–357. [[CrossRef](#)]
23. LeTerrier, J.; Maury, R.C.; Thonon, P.; Girard, D.; Marchal, M. Clinopyroxene compositions as a method of identification of the magmatic affinities of paleovolcanic series. *Earth Planet. Sci. Lett.* **1982**, *59*, 139–154. [[CrossRef](#)]
24. Hamm, H.-M.; Vieten, K. Zur Berechnung der Kristallchemischen Formel und des Fe³⁺ Gehaltes von Klinopyroxen aus Elektronenstrahl-Mikroanalysen. *Neues Jahrb. Mineral. Mh.* **1971**, *7*, 310–314.
25. Thompson, J.B. Role of aluminium in the rock-forming silicates (abst.). *Geol. Soc. Am. Bull.* **1947**, *58*, 1232.
26. Chivas, A.R. Geochemical evidence for magmatic fluids in porphyry copper mineralization. Part I. Mafic silicates from the Koloula Igneous Complex. *Contrib. Mineral. Petrol.* **1981**, *78*, 389–403. [[CrossRef](#)]
27. Yamaguchi, Y. Hornblende-cummingtonite and hornblende-actinolite intergrowths from the Koyama calc-alkaline intrusion, Susa, southwest Japan. *Am. Mineral.* **1985**, *70*, 980–986.

28. Zingg, A.J. Intra- and intercrystalline cation-exchange reactions in zoned calcic amphibole from the Bushveld complex. *Can. Mineral.* **1993**, *31*, 649–663.
29. Czamanske, G.K.; Wones, D.R. Oxidation during magmatic differentiation, Finnmarka, Oslo area, Norway: Part 2, The mafic silicates. *J. Petrol.* **1973**, *14*, 349–380. [[CrossRef](#)]
30. Helmy, H.M.; Ahmed, A.F.; El Mahallawi, M.M.; Ali, S.M. Pressure, temperature and oxygen fugacity conditions of calc-alkaline granitoids, Eastern Desert of Egypt, and tectonic implications. *J. Afr. Earth Sci.* **2004**, *38*, 255–268. [[CrossRef](#)]
31. Green, D.H.; Mysen, B.O. Genetic relationship between eclogite and hornblende+ plagioclase pegmatite in western Norway. *Lithos* **1972**, *5*, 147–161. [[CrossRef](#)]
32. Sisson, T.W.; Grove, T.L.; Coleman, D.S. Hornblende gabbro sill complex at Onion Valley, California, and a mixing origin for the Sierra Nevada batholith. *Contrib. Mineral. Petrol.* **1996**, *126*, 81–108. [[CrossRef](#)]
33. Jahns, R.H. Internal evolution of pegmatite bodies. In *Granitic Pegmatites in Science and Industry*; Mineralogical Association of Canada Short Course Handbook 8; Černý, P., Ed.; Mineralogical Association of Canada: Quebec City, QC, Canada, 1982; pp. 293–327.
34. Mysen, B. Water-melt interaction in hydrous magmatic systems at high temperature and pressure. *Prog. Earth Planet. Sci.* **2014**, *1*, 4. [[CrossRef](#)]
35. Murphy, J.B. Appinite suites: A record of the role of water in the genesis, transport, emplacement and crystallization of magma. *Earth-Sci. Rev.* **2013**, *119*, 35–59. [[CrossRef](#)]
36. Hanley, J.J.; Gladney, E.R. The presence of carbonic-dominant volatiles during the crystallization of sulfide-bearing mafic pegmatites in the North Roby Zone, Lac des Iles Complex, Ontario. *Econ. Geol.* **2011**, *106*, 33–54. [[CrossRef](#)]
37. London, D.; Morgan, G.B. The pegmatite puzzle. *Elements* **2012**, *8*, 263–268. [[CrossRef](#)]
38. Laumonier, M.; Gaillard, F.; Muir, D.; Blundy, J.; Unsworth, M. Giant magmatic water reservoirs at mid-crustal depth inferred from electrical conductivity and the growth of the continental crust. *Earth Planet. Sci. Lett.* **2017**, *457*, 173–180. [[CrossRef](#)]
39. Grove, T.L.; Till, C.B.; Krawczynski, M.J. The role of H₂O in subduction zone magmatism. *Annu. Rev. Earth Planet. Sci.* **2012**, *40*, 413–439. [[CrossRef](#)]
40. Collins, W.J.; Murphy, J.B.; Johnson, T.E.; Huang, H.Q. Critical role of water in the formation of continental crust. *Nat. Geosci.* **2020**, *13*, 331–338. [[CrossRef](#)]
41. Castro, A.; Corretge, L.G.; De la Rosa, J.D.; Fernandez, C.; Lopez, S.; Garcia-Moreno, O.; Chacon, H. The appinite–migmatite complex of Sanabria, NW Iberian massif, Spain. *J. Petrol.* **2003**, *44*, 1309–1344. [[CrossRef](#)]
42. Lledo, H.L.; Jenkins, D.M. Experimental investigation of the upper thermal stability of Mg-rich actinolite; implications for Kiruna-type iron deposits. *J. Petrol.* **2008**, *49*, 225–238. [[CrossRef](#)]

Publisher’s Note: MDPI stays neutral with regard to jurisdictional claims in published maps and institutional affiliations.



© 2020 by the author. Licensee MDPI, Basel, Switzerland. This article is an open access article distributed under the terms and conditions of the Creative Commons Attribution (CC BY) license (<http://creativecommons.org/licenses/by/4.0/>).